

Pattern Formation in a Rotating Aqueous Suspension

A. P. J. BREU, C. A. KRUELLE and I. REHBERG

Experimentalphysik V, Universität Bayreuth, D-95440 Bayreuth, Germany

PACS. 45.70.Mg – Granular flow: mixing, segregation and stratification.

PACS. 45.70.Qj – Pattern formation.

PACS. 05.65.+b – Self-organized systems.

Abstract. – A novel pattern forming instability in a mixture of a granular material and water in a horizontal rotating drum is experimentally investigated. The particles accumulate in radial symmetric rings separated by pure water. The transition between the homogeneous state and the structured state is hysteretic. The transition point is extrapolated from the growth rates of the chain of rings. The trajectory of a single particle is discussed to estimate an upper boundary for the transition point.

Introduction. – Granular media show an interesting and peculiar dynamic behavior [1], and are also of major importance in technological processes. One of the standard problems of the powder technology is the mixing of materials [2]. It is often accompanied by pattern formation like stratification [3] or segregation [4, 5, 6, 7]. The axial and radial segregation in rotating-drum mixers with dry multicomponent mixtures, like small and large particles or particles of different densities, has been investigated. The different angles of repose of the two species are considered as the segregation mechanism for the axial segregation. The separation of large and small particles has recently been observed in a mixture of particles dispersed in a lower density fluid [8]. In the presence of a fluid the time for the pattern formation is significantly decreased.

Granular media immersed in a fluid show a type of segregation even for monodisperse particles [9, 10, 11, 12]. The volume fraction of granular particles in these experiments is much less than in the previous cases. Furthermore, the driving frequency of the drum is sufficiently high for the centrifugal forces to become dominant. The observed pattern is a chain of circumferential rings of high particle concentration. Tirumkudulu *et al.* reported on this type of axial segregation in partially filled horizontal cylinders [9, 11]. In both cases they used suspensions of particles, which were neutrally buoyant. If the device was completely filled with the suspension, no instability was observed at all. The experiment was modeled theoretically by Govindarajan *et al.* [13] including shear-induced diffusion of particles, concentration-dependent viscosity and the existence of a free surface. Boote and Thomas [10], and Thomas *et al.* [12] reported similar experiments with particle densities less and more dense than the surrounding fluid in a partially fluid-filled cylinder. For particles of a different density than the fluid, the free surface is not necessary for the instability. Lipson observed this phenomenon during crystal growth in a supersaturated solution [14].

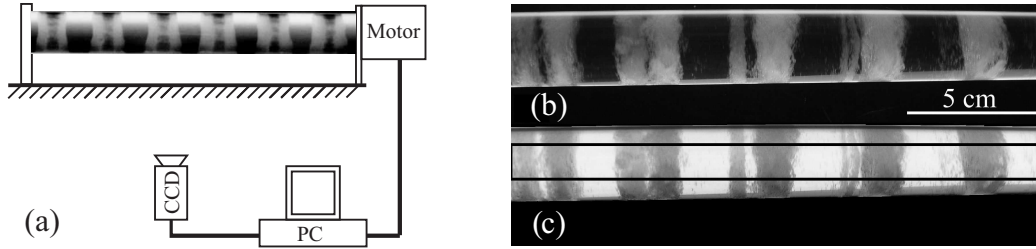


Fig. 1 – (a) Experimental setup. (b) Photograph of the tube with the pattern. A top view of the tube is shown. The sand is accumulated in the white areas. (c) Corresponding transmitted light intensity, sand accumulations appearing dark. The 5 pixel wide frame indicates the area considered for further analysis.

In this publication we present experiments on axial segregation of monodisperse particles which have a higher density than the surrounding fluid. The experiments have been carried out in a drum, which was completely filled with a sand-water mixture. We estimate an upper boundary for the critical frequency for the onset of the pattern formation by the numerical analysis of the trajectory of a single particle.

Experiments. – The experimental setup is shown schematically in Fig. 1(a). The experiment consists of a horizontally aligned plexiglass tube, which is 400 mm long. Its inner diameter measures 23.73 ± 0.05 mm. Both ends are closed with plexiglass plugs. The tube is filled with 2.5% (by volume) glass beads and 97.5 % water. This is sufficient to reach about 85% of the close packing for a monolayer on a cylindrical surface. The glass beads are ballotini impact beads with a density of 2.45 g cm^{-3} and diameters between $280 \mu\text{m}$ to $300 \mu\text{m}$.

One end of the tube is attached rigidly to a dc-motor, which rotates the tube around its cylinder axis. The motor speed is controlled with an accuracy of 10^{-4} . The control unit allows rotation frequencies f_{rot} from 0 Hz to 50 Hz in steps of $\frac{1}{60}$ Hz with a maximal acceleration of 1047 s^{-2} . The axial sand distribution in the tube is measured via light transmission, with a neon light placed behind the tube. A CCD camera, connected to a frame grabber, detects the intensity of the transmitted light. Each frame consists of a narrow strip (512×5 pixels) along the tube displaying high sand concentrations as dark stripes in a bright surrounding (Fig. 1(b) and (c)).

The experimental protocol consists of a stepwise increase or decrease of the rotation frequency from 2.4 Hz to 4.0 Hz followed by a subsequent waiting period of 5 min, after which transients have disappeared. No patterns are visible for high frequencies above 3.9 Hz and frequencies below 2.9 Hz (Fig. 2(a) and (b)). At intermediate frequencies patterns appear, depending on the history of the system. Thus we display the intensities for increasing and decreasing rotation frequencies in part (a) and (b) of Fig. 2.

Alternatively we characterize the pattern by a discrete Fourier decomposition of the lines (Fig. 2). As soon as the rings appear, well defined peaks show up in the power spectrum. In the case of decreasing rotation frequencies the first peak is located at $q_{\text{low}} = 1.49 \pm 0.05 \text{ cm}^{-1}$, which corresponds to a ring spacing of $4.23 \pm 0.15 \text{ cm}$. For frequencies below 3.5 Hz the first peak almost vanishes and a peak at $q_{\text{high}} = 3.19 \pm 0.05 \text{ cm}^{-1}$ becomes dominant, due to a splitting of the rings. The pattern returns to q_{low} for frequencies between 3.4 Hz and 3.25 Hz. Below 3.25 Hz the particles start to accumulate at the right hand side of the tube. Whether the system chose the right or the left side could not be predicted in advance. For rotation frequencies below 2.9 Hz the sand distributed again homogeneously in the tube. Increasing

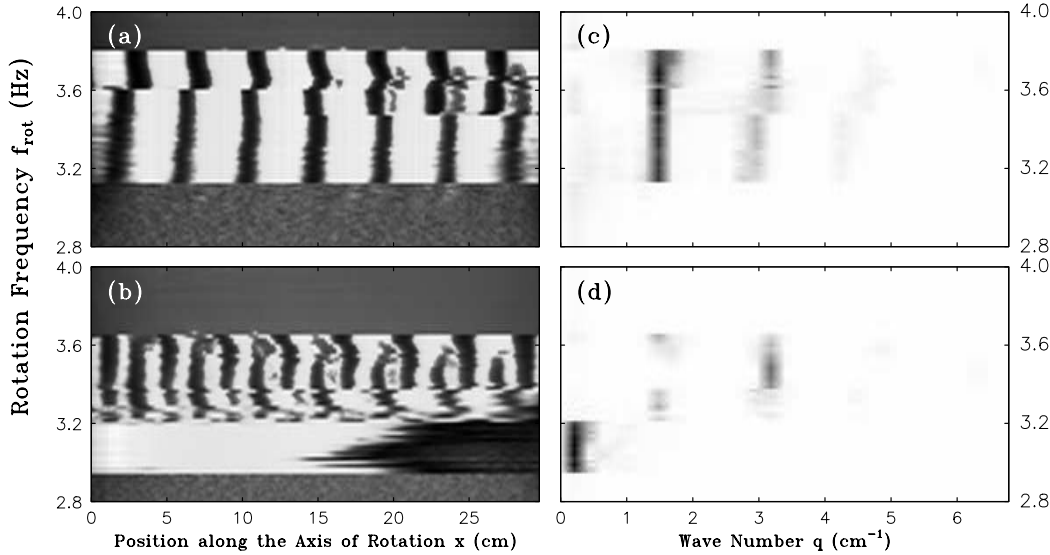


Fig. 2 – Different patterns at quasistatic changes of the (a) increasing and (b) decreasing rotation frequencies. Each line corresponds to one measurement of the sand distribution along the axes of rotation, which is an average of 20 images taken within 0.8 s. These intensities are normalized by the intensities obtained at zero rotation frequency, in order to prevent errors due to inhomogeneous illumination. The lines are plotted with an offset proportional to the rotation frequency to show the evolution of the system. The frequency was swept between 2.4 Hz and 4.0 Hz. (c) and (d) show the corresponding power spectra for increasing and decreasing rotation frequencies. Each line of (a) and (b) was transformed and plotted by the same offset as before.

the rotation frequency leads to a different scenario as shown in Fig. 2(a) and 2(c). There the characteristic ring spacing is almost constant at q_{low} . No accumulation at a tube end was observed even after waiting periods of 30 min.

To get a more precise picture of the transition points, we take as an order parameter the root mean square A_{rms} of the measured intensities along the axes of rotation (Fig. 3). We observe two hysteresis loops, which are related to the transitions between structured and unstructured states. These hysteresis loops indicate that the transitions can be considered as subcritical bifurcations.

In order to characterize the bifurcation around 3.7 Hz further we now concentrate on the temporal evolution of the instability. We assume

$$\partial_t A = \sigma A \quad (1)$$

where A describes the amplitude for a given wave number of the pattern, and σ the growth rate. To measure σ as a function of the driving frequency we start at a rotation frequency, where the granular medium forms a homogeneous layer ($f_{\text{rot}} = 4$ Hz). Then we decelerate the motor suddenly to a frequency where the ring pattern is stable ($f_{\text{rot}} < f_{\text{rot},c}$). Due to this sudden change, the pattern will grow in time, as described by equation (1) to lowest order. Figure 4 shows the growth of the amplitude in time after a jump from 4.0 Hz to 3.583 Hz (Fig. 4(b)), and to 3.550 Hz (Fig. 4(a)). The amplitude in this plot was obtained from the power spectrum by selecting the mode $q_{\text{low}} = 1.49 \text{ cm}^{-1}$, which is the first stable one if the rotation frequency is decreased quasistatically (see Fig. 2(d)). The solid line is the fit of an

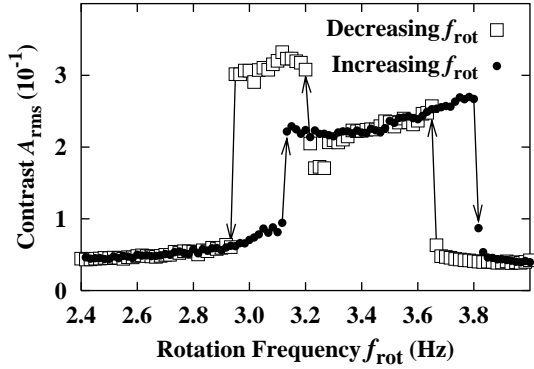


Fig. 3 – Amplitude of the pattern as a function of the rotation frequency.

exponential function to the data. At higher amplitudes the growth is no longer exponential. In fact, the amplitudes decay after 100 s (Fig. 4(a)). This non-monotonic effect is caused by a rearrangement of the pattern towards a higher wave number.

This quenching of the system was performed for final rotation frequencies between 3.4 Hz and 3.9 Hz. Above 3.65 Hz no growth of the pattern was observed within a measurement time of 5 minutes. Below 3.4 Hz it was not possible to measure a growth rate for q_{low} . For frequencies between 3.633 Hz and 3.567 Hz the final stable mode was q_{low} . At lower frequencies

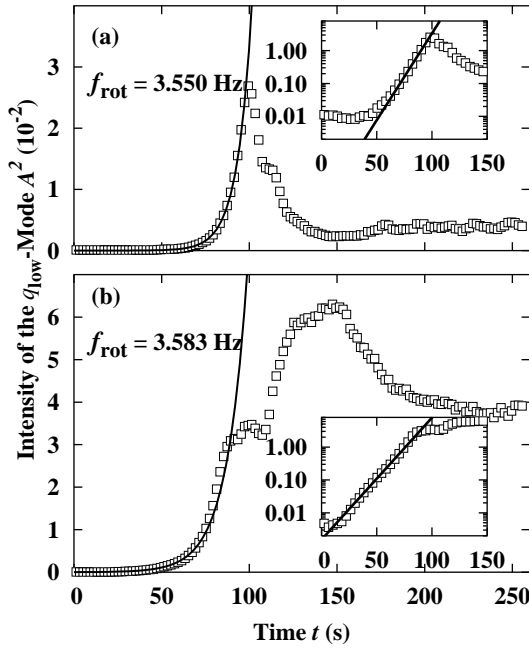


Fig. 4 – Growth of the amplitude of the pattern as a function of time for two different rotation frequencies. The solid line represents the fit of an exponential function to the data. The insets show the regions of exponential growth on a semi-logarithmic scale.

this mode first grew in time and decayed afterwards, being replaced by the higher stable mode q_{high} . Nevertheless, it was also possible to extract a growth rate for these frequencies, but with less accuracy, as indicated by the error bars in Fig. 5.

All measured growth rates are plotted as a function of the rotation frequency in Fig. 5. For f_{rot} between 3.55 Hz and 3.65 Hz the growth rate of the mode q_{low} increases roughly linearly with decreasing frequency, and saturates around 3.4 Hz, due to the different stable mode q_{high} , as seen in Fig. 4(a). To model the increasing growth rate as well as the saturation, we fitted a parabola to the data. This parabola was then used to extrapolate the data for $\sigma \rightarrow 0$. The corresponding critical rotation frequency is $f_{\text{rot},c} = 3.641 \pm 0.035$ Hz.

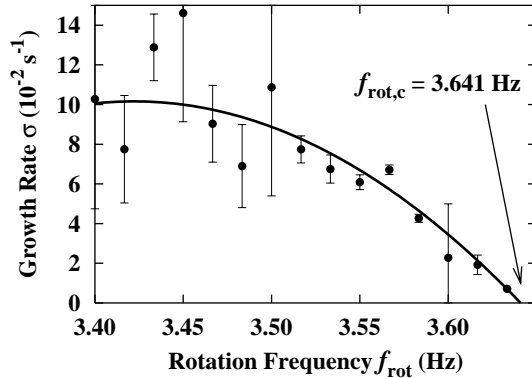


Fig. 5 – Growth rate as a function of driving frequency f_{rot} .

Discussion and conclusion. – In order to estimate an upper boundary for the critical rotation frequency $f_{\text{rot},c}$ we analyze the motion of a single particle in the laboratory frame, neglecting the interaction with the neighboring particles. The calculation estimates the frequency for the detachment of a particle from the wall, which is a necessary, but not a sufficient criterion for pattern formation. A complete understanding of the instability cannot be achieved by this simple calculation. At high rotation frequencies the suspension is in rigid body rotation, and the particle sticks to the inner wall of the tube. Below a critical frequency the particle detaches from the wall and falls on a parabola-like trajectory described by the equation of motion

$$m\ddot{\mathbf{x}} = \mathbf{F}_{\text{G,res}} + \mathbf{F}_{\text{S}} + \mathbf{F}_{\text{cb}}. \quad (2)$$

$\mathbf{F}_{\text{G,res}}$ represents the force of gravity, reduced by buoyancy:

$$\mathbf{F}_{\text{G,res}} = \frac{4}{3}\pi r^3 (\rho_p - \rho_f) \mathbf{g}. \quad (3)$$

r is the radius of the particle, ρ_p and ρ_f are the density of the particle and the fluid, respectively. The drag of the fluid on the particle is modelled by a modified Stokes formula

$$\mathbf{F}_{\text{S}} = -6\pi\eta r (\mathbf{v}_p - \mathbf{v}_f) \cdot \lambda, \quad (4)$$

where η denotes the dynamic viscosity of the fluid. \mathbf{v}_p and \mathbf{v}_f are the velocity of the particle and the fluid, respectively, at the position of the particle. For the fluid velocity \mathbf{v}_f we assume that the fluid is in rigid body rotation. Since the particle velocity is approximately equal to the fluid velocity, the Reynolds number is close to zero. λ is the correction of the Stokes

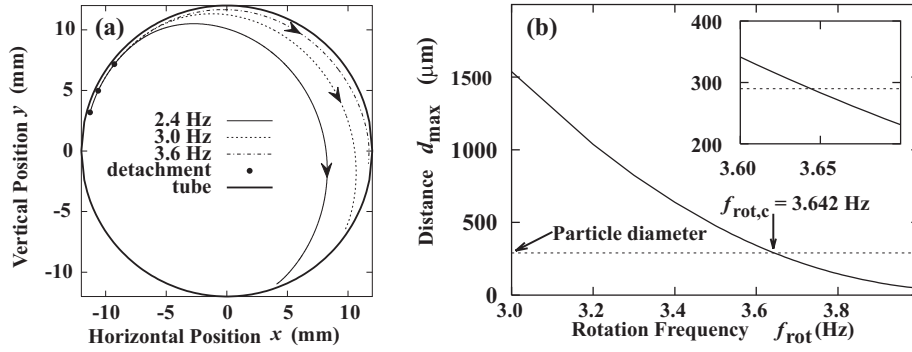


Fig. 6 – (a) Trajectories of a particle falling in a viscous fluid for different rotation frequencies. The fluid is assumed to perform a rigid body rotation. (b) Maximal distance to the tube wall of a particle falling in a viscous fluid as a function of rotation frequency. The dashed line is drawn at the particle diameter. The inset is a close-up of the critical region.

formula for particles close to the wall, derived by Brenner for vanishing Reynolds number [15]:

$$\lambda = \frac{4}{3} \sinh \alpha \sum_{n=1}^{\infty} \frac{n(n+1)}{(2n-1)(2n+3)} \times \left[\frac{2 \sinh(2n+1)\alpha + (2n+1) \sinh 2\alpha}{4 \sinh^2(n+\frac{1}{2})\alpha - (2n+1)^2 \sinh^2 \alpha} - 1 \right], \quad (5)$$

where the particle radius dependence which is taken care of by α is defined as

$$\alpha = \cosh^{-1} \left(\frac{d+r}{r} \right). \quad (6)$$

d is the distance of the sphere's surface to the wall.

The third force is caused by the radial pressure distribution of the fluid in rigid body rotation:

$$\mathbf{F}_{\text{cb}} = -\frac{4}{3}\pi r^3 \rho_f \omega^2 \mathbf{x}, \quad (7)$$

the centrifugal buoyancy [16].

While the detachment point can be calculated analytically [17], the path of the particle is obtained by numerical integration of the equation of motion (2). Note that the particle, at the detachment point, has a distance of $\tilde{R} = R - r - \delta$ from the center of the tube. R is the inner radius and δ the surface roughness of the tube. It is necessary to include the surface roughness, since the wall correction (5) becomes singular for vanishing distance d . We have chosen $\delta = 1 \mu\text{m}$, which is a typical value for cast processes.

Starting from the detachment point, we integrate the equation of motion (2) until the particles touched the wall of the tube again. Three different trajectories are shown in Fig. 6(a). From these trajectories we calculate the distance of the particle from the tube wall as a function of time. Each curve has a unique maximum d_{\max} , which depends on the rotation frequency of the tube. We determined numerically this maximal distance for different rotation frequencies (Fig. 6(b)). For the rearrangement of the particles, which initially tend to form a close packed monolayer, into separated rings, some individual particles have to jump over their neighbors. In order to do this they have to achieve at least a distance d_{\max} equal to one particle diameter. If the distance is less than the diameter, particles will not be able to pass their neighbors. Therefore the critical frequency is found at the distance d_{\max} equal to one particle diameter

2r. By this we obtain a critical rotation frequency of 3.642 ± 0.060 Hz, which is in agreement with the experimental value of 3.641 ± 0.035 Hz.

A detailed theoretical investigation of the interaction between sand and water leading to the ring pattern remains to be done. A two-fluid approach might be difficult, since the primary flow is not trivial [18]. A molecular-dynamics simulation [19], taking into account both the trajectories of the grains and the fluid flow, seems to be more promising.

We like to thank S. Aumaître, V. Frette, and M.A. Scherer for many interesting and inspiring discussions. This work has been supported by the Deutsche Forschungsgemeinschaft RE-588/12.

REFERENCES

- [1] H.M. Jaeger, S.R. Nagel, and R.P. Behringer. Granular solids, liquids, and gases. *Rev. Mod. Phys.*, 68(4):1259–1273, 1996.
- [2] Kei Miyamoto. Mixing. In K. Gotoh, H. Masuda, and K. Higashitani, editors, *Powder Technology Handbook*, chapter V, pages 609–625. Marcel Dekker, 2nd edition, 1997.
- [3] H.A. Makse, S. Havlin, R.P. King, and H.E. Stanley. Spontaneous stratification in granular mixtures. *Nature*, 386:379–382, 1997.
- [4] V. Frette and Joel Stavans. Avalanche-mediated transport in a rotated granular mixture. *Phys. Rev. E*, 56(6):6981–6990, 1997.
- [5] K.M. Hill and J. Kakalios. Reversible axial segregation of binary mixtures of granular materials. *Phys. Rev. E*, 49(5):R3610–R3613, 1994.
- [6] C.M. Dury and G.H. Ristow. Axial particle diffusion in rotating cylinders. *Granular Matter*, 1:151–161, 1999.
- [7] D.V. Khakhar, J.J. McCarthy, and J.M. Ottino. Radial segregation of granular mixtures in rotating cylinders. *Phys. Fluids*, 9(12):3600–3614, 1997.
- [8] N. Jain, D.V. Khakhar, R.M. Lueptow, and J.M. Ottino. Self-organization in granular slurries. *Phys. Rev. Lett.*, 86(17):3771–3774, 2001.
- [9] M. Tirumkudulu, A. Tripathi, and A. Acrivos. Particle segregation in monodisperse sheared suspensions. *Phys. Fluids*, 11(3):507–509, 1999.
- [10] O.A.M. Boote and P.J. Thomas. Effects of granular additives on transition boundaries between flow states of riming flows. *Phys. Fluids*, 11(8):2020–2029, 1999.
- [11] M. Tirumkudulu, A. Mileo, and A. Acrivos. Particle segregation in monodisperse sheared suspensions in a partially filled rotating horizontal cylinder. *Phys. Fluids*, 12(6):1615–1618, 2000.
- [12] P.J. Thomas, G.D. Riddell, S. Kooner, and G.P. King. Fine structure of granular banding in two-phase rimming flow. *Phys. Fluids*, 13(9):2720–2723, 2001.
- [13] R. Govindarajan, P.R. Nott, and S. Ramaswamy. Theory of suspension segregation in partially filled horizontal rotating cylinders. *Phys. Fluids*, 13(12):3517–3520, 2001.
- [14] S.G. Lipson. Periodic banding in crystallization from rotating supersaturated solutions. *J. Phys.: Condens. Matter*, 13:5001–5008, 2001.
- [15] H. Brenner. The slow motion of a sphere through a viscous fluid toward a plane surface. *Chem. Eng. Sci.*, 16:242–251, 1961.
- [16] G.K. Batchelor. *An Introduction to Fluid Dynamics*. Cambridge University Press, 1967.
- [17] A.P.J. Breu (unpublished). *Segregation und Strukturbildung in granularer Materie*. PhD thesis, Universität Bayreuth, Experimentalphysik V, Universität Bayreuth, 95440 Bayreuth, 2003.
- [18] A. Lange and A. Engel. Private communications.
- [19] W. Kalthoff, S. Schwarzer, and H. J. Herrmann. Algorithm for the simulation of particle suspensions with inertia effects. *Phys. Rev. E*, 56(2):2234–2242, 1997.